Final Report

On

The Effects of Externally Solidified Product on Wave Celerity and Quality of Die Cast Products

US Department of Energy Grant/Contract No.
DE-FC07-99ID13844

OSURF Project No. 739694

Report Period: 07-03-2000 through 07-02-2003

Principal Investigators:
Carroll Mobley, Yogeshwar Sahai, and Jerry Brevick
The Ohio State University

September 5, 2003

Final Report

On

The Effects of Externally Solidified Product on Wave Celerity and Quality of Die Cast Products

Background

The cold chamber die casting process is used to produce essentially all the die cast aluminum products and about 50% of the die cast magnesium products made today. Modeling of the cold chamber die casting process and metallographic observations of cold chamber die cast products indicate that typically 5 to 20 % of the shot weight is solidified in the shot sleeve before or during cavity filling. The portion of the resulting die casting which is solidified in the shot sleeve is referred to as externally solidified product, or, when identified as a casting defect, as cold flakes. The externally solidified product significantly influences

1. the wave celerity and gas entrapment during the slow shot stage of the process,
2. the fluidity of the alloy and its ability to completely fill the die cavity,
3. the microstructure of the resulting die casting, and
4. the mechanical properties of the resulting die casting.

This project was directed to extending the understanding of the effects of externally solidified product on the cold chamber die casting process and products to enable the production of defect-free die castings and reduce the energy associated with these products. The projected energy savings from controlling the fraction of externally solidified product in die cast components is 40 x 10^{12} Btu through the year 2025.

Approach

The project involved three parallel activities:

1. Physical analog modeling with aqueous solutions under
    a. isothermal conditions with a second phase initially present on the shot sleeve wall, and
    b. athermal conditions with solidification in transparent shot sleeves,
2. Computer modeling both the physical analog systems and aluminum die casting systems, and
3. Evaluating the quality of cold chamber die cast aluminum alloy components produced under controlled and monitored conditions with relatively small and large fractions of externally solidified products.

Project Activities and Accomplishments

The activities performed during the third year of this project were in keeping with those defined in the Work Statement submitted at the beginning of the project. Those activities were to:

1. Conduct Athermal Transparent Shot Sleeve Experiments to Determine Effects of Externally Solidified Phase on Wave Formation and Air Entrapment.

2. Develop and Evaluate the Computer Modeling of the Shot Sleeve Section of the Cold Chamber Die Casting System.

3. Determine the Effect of the Fraction Externally Solidified Phase(s) on the Tensile And Fatigue Properties of the Die Cast Aluminum Components (C&D).

4. Prepare and Submit Third Annual & Final Project Report

This final report contains the results of the third year of the study and the overall conclusions formulated from all three years of activity.

Isothermal and Athermal Transparent Shot Sleeve Activities

As described in the Second Annual Report for the project, OSU's Center for Die Casting has a transparent shot sleeve system which was originally designed and build by Prince Machine Corporation. The Prince transparent shot sleeve system allows experimentation on the fluid flow and wave formation of transparent analog fluids to physically simulate the fluid flow phenomena which occur with liquid aluminum alloys in cold chamber die casting systems. A picture of the Prince transparent shot sleeve system is shown in Figure 1. The Prince transparent shot sleeve system consists of (1) a 2000 psi (13.8 Mpa) hydraulic pump, (2) a plunger rod and attached plunger tip, (3) a transparent polymethylmethacrylate (PMMA) sleeve, (4) a die cavity or appropriate liquid collection chamber, and (5) a Visi-Trak plunger position-time controlling and monitoring unit. The plunger rod is a 1.25 inch diameter, 30 inch long, steel rod. The plunger tip is attached to the plunger rod and has an outer diameter slightly less than the inside diameter of the selected shot sleeve. A liquid seal is maintained between the plunger tip and the shot sleeve with two neophere O-rings fitted in diametrical grooves on the plunger tip. The Visi-Trak controlling and monitoring system
is connected to the plunger rod . The Visi-Trak operates a servo valve and control valve to control the position, velocity, and acceleration of the plunger.

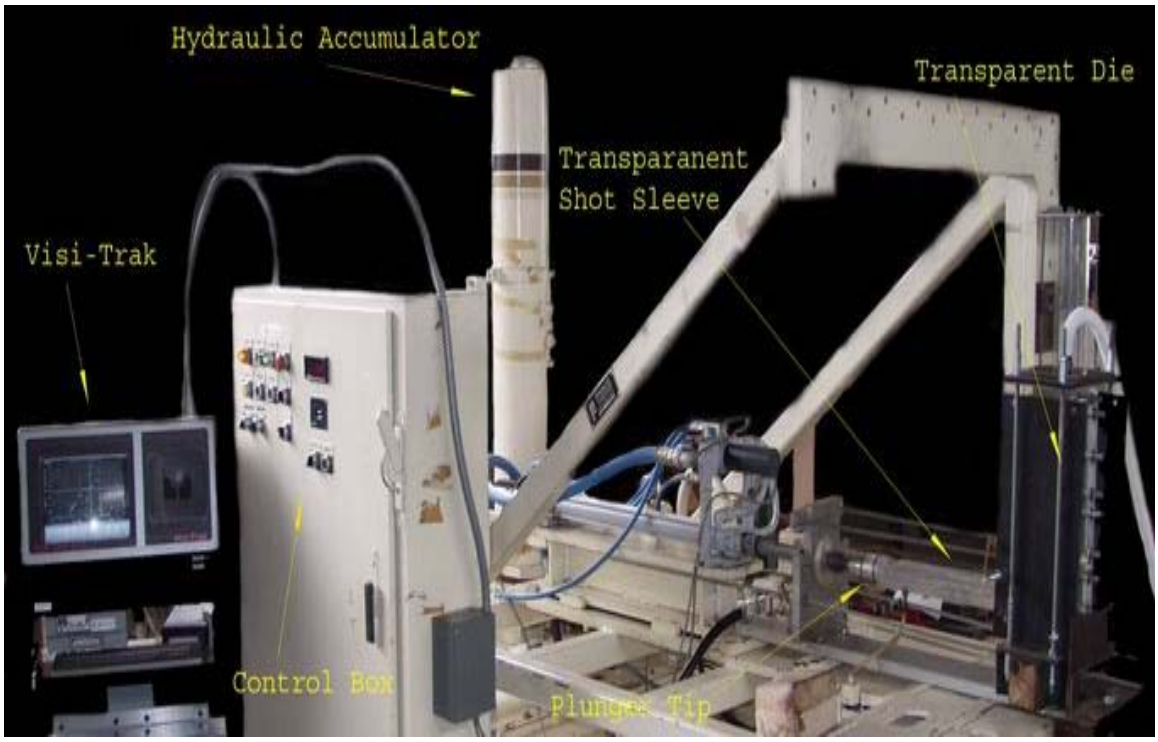

Figure 1: Photograph of the Prince Transparent Shot Sleeve System

Transparent PMMA shot sleeves can be selected between 2 and 4 inches inner diameter with one-quarter inch wall thickness. The shot sleeves are typically 20.25 inches in length. Located on the top of the shot sleeve near the near the plunger rod initial position is a 1.7 inch diameter pour hole. The shot sleeve contained volumes range from 63.62 cubic inches for the 2 inch inner diameter shot sleeve to 254.47 cubic inches for the 4 inch inner diameter shot sleeve. The Visi-Trak controller can be programmed to provide different shot profiles (plunger position-time histories). Programming consists of entering designated plunger velocities and accelerations at up to 6 positions during the plunger movements. Shot profiles can be obtained using open and closed loop systems. Velocity is expressed as an integer (in/sec) in a closed loop profile, but is expressed as a percentage of the valve opening (%) during open loop profiles.

The Prince transparent shot sleeve system is used to simulate molten metal die cast systems using a room temperature or near room temperature analog fluid, such as water or water-glycerin solutions. Shot sleeve filling, plunger movement and wave formation, and die filling, are recorded using a Kodak Ektapro HS Motion Analyzer High-Speed Camera Model 4540. The camera is capable of recording up to 4500 frames per second with full field viewing is used. A greater framing rate (i.e. frames per second) can be achieved with a narrowed field of vision. Up to 1000 frames are recorded onto S-VHS tapes. The Kodak Ektapro HS Model 4540 camera is limited to black and white images.

The type of liquid used to physically simulate the molten alloys used in die casting is selected to have similar physical properties to the liquid alloy to be studied. Similarity is based on equivalent or near equivalent, Reynolds number ($\rho vd/\eta$), Weber number ($\sigma/\sqrt{\rho vd}$), and Prandtl number ($\eta c/k$). The Prince transparent shot sleeve system has been used primarily as an isothermal (uniform room temperature) system and the waves formed for the various shot profiles have not included any effects of the externally solidified product (ESP) formed within an athermal and actual die casting shot sleeve system. The Prince transparent shot sleeve system was modified to allow heat transfer from the liquid to the shot sleeve and allow solid to form along the interior of the shot sleeve, thereby simulating the formation and effects of the ESP.

Athermal Transparent Shot Sleeve Cooling System

Figure 2 is a schematic illustration of the cooling system for the athermal transparent Prince shot sleeve on the Prince system. A half cylinder of PMMA was placed under the shot sleeve to serve as a trough for liquid nitrogen, the system coolant. Liquid nitrogen was poured into the trough to cool the bottom portion of the PMMA shot sleeve. Ice particles form as water is placed inside the shot sleeve. Ammonium chloride crystals form when the hyper-eutectic water-30 weight percent ammonium chloride solution is used. The cooling sleeve is 19.5 inches long and have an inner diameter of 3" and outside diameter of 3.5". Each end of the cooling sleeve contains another piece of PMMA to prevent liquid nitrogen from escaping. The cooling jacket was mechanically attached to the transparent shot sleeve without interfering with the motion of the plunger rod or reducing the visibility of the resultant wave formation. Experiments to evaluate and confirm the acceptability of using PMMA as the shot sleeve and liquid nitrogen coolant containing material were conducted as part of the second and third year's project activities.

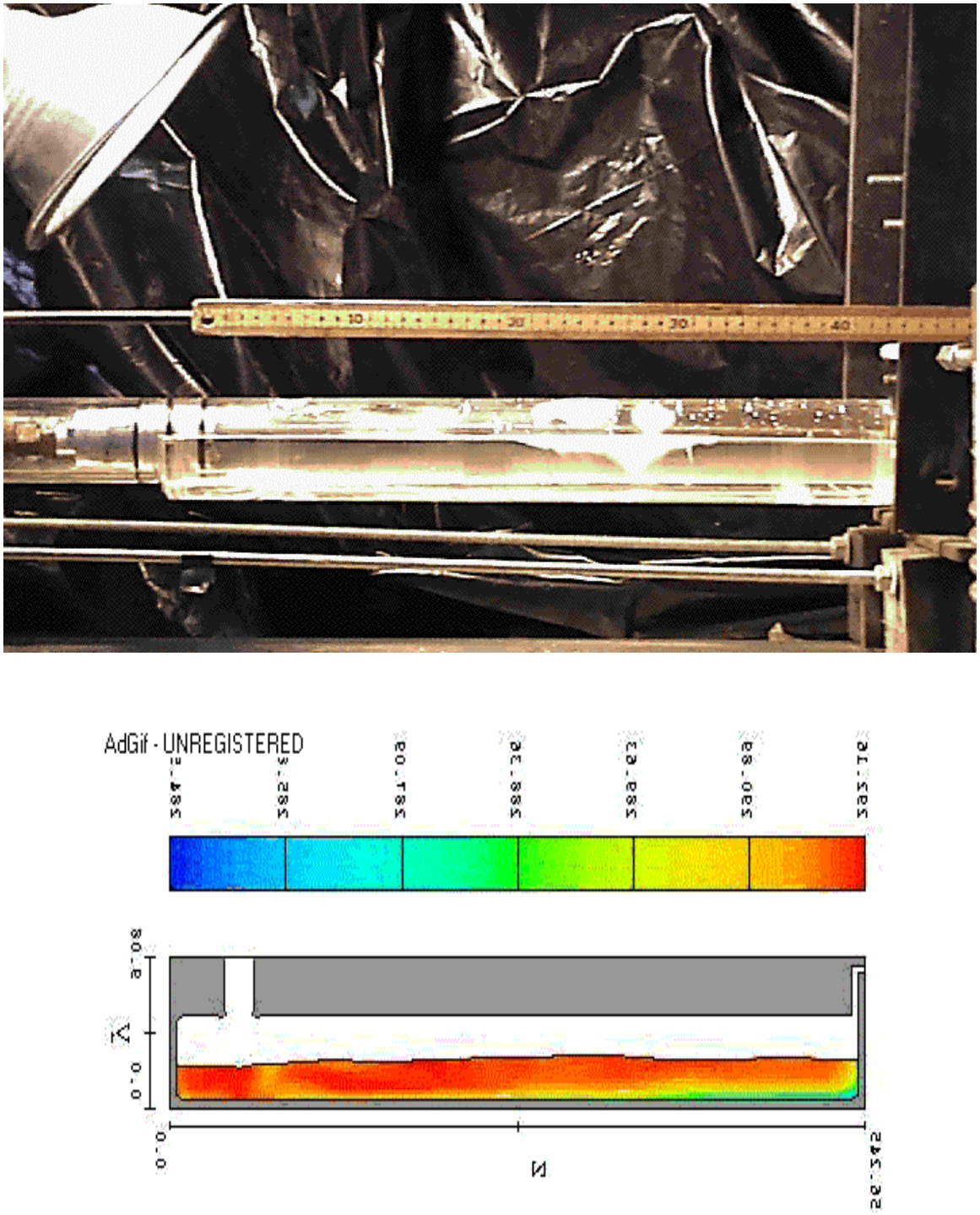

Figure 2: Wave Formation in the Athermal Transparent Shot Sleeve with Water-30 weight % Ammonium Chloride Solution

A comparison of the wave dynamics for the isothermal and athermal transparent shot sleeve systems for the critical plunger velocity with water and the hyper-eutectic

water-ammonium chloride solution was made. The primary solidification products (ice in the case of water and ammonium chloride crystals in the case of the hyper-eutectic water ammonium chloride solution) formed in all of the athermal experiments. However, in keeping with the low Prandtl numbers associated with the transparent analog systems as compared with aluminum-based alloys, the liquids had to be cooled for significantly longer times to form an equivalent fraction of solid. The aqueous-based transparent liquid were allowed to dwell in the cooled PMMA shot sleeves for several minutes to form a layer of solid on the shot sleeve with a volume fraction of 0.05 to 0.1. Dwell times of the order of several to tens of seconds will produce equivalent fraction of solids in aluminum-based alloys in H-13 steel shot sleeves. Flow3D computer simulations produced similar fraction solid-time curves for the aqueous solutions in the liquid nitrogen cooled PMMA shot sleeves. A comparison of the atheraml wave formation with the water-30 weight % ammonium chloride solution in the transparent shot sleeve and the Flow3D computer simulations for the same system are included in Figure 2.

For equivalent plunger velocities, the waves formed in the isothermal and athermal systems were nearly identical, indicating that the formation and incorporation of the ESP does not play a major rule in the wave form. However, it was noted in the Prince shot sleeve experiments, as in the Briggs & Stratton aluminum die casting experiments, that the formation of solid on the shot sleeve wall may significantly influence the plunger position-time record. The solid shell formed along the lower portion of the shot sleeve acts as a solid hemispherical shell. As the thickness of the shell increases, the force required to collapse the shell also increases. Thus, the presence of the solidified shell on the shot sleeve requires that a greater pressure be applied to the plunger to allow it to move with the same velocity it would have when no solid shell were present. When the shell thickness becomes too large, the force required to deform and collapse the solid shell may exceed the available pressure in the system used to move the plunger.

Flow 3D Computer Modeling Activities

Computer simulations of the 2-dimensional and three dimensional shot sleeve systems using the Flow 3D computer program were continued throughout this report period. ZZZ Flow 3D simulations were performed during the third year of this project. The major computational activity was to introduce the athermal conditions in the shot sleeve and compare the athermal wave formation results with the previously reported isothermal results. Figure XX provides a comparison of the computed wave dynamics for water in a 2-dimensional channel under isothermal and athermal conditions. These computer results include turbulence and surface energy effects. The preliminary finding associated with the computer modeling is that the heat transfer plays only a minor effect in the formation and dynamics of the fluid wave in the shot sleeve. The computer results, and the findings of the Briggs & Stratton aluminum die casting campaign, suggest that the effect of the ESP is more a mechanical effect, altering the plunger velocity in association with the buckling or mechanical influence of the ESP on the plunger motion. The computer models developed to date assume that the plunger history is independent of the ESP formation.

Effect of ESP on Mechanical Properties of Aluminum Alloy Die Castings

A second die casting campaign was conducted at Briggs & Stratton Corp. in Milwaukee, WI on February 27, 2003. The primary objective of the February 27th B&S die casting campaign was to produce aluminum alloy die castings with varying amounts of externally solidified product (ESP) for future characterization in keeping with the DOE project objectives. This section summarizes the die casting conditions used to produce those samples and the tensile properties found in the samples.

Part Description and Machine Setup

The die castings produced in this campaign were tensile bars with inner diameters of 0.5, 0.375, and 0.25 inches. An example of the castings produced is shown in Figure 3.

Figure 3: Part Illustration

The tensile bars in the campaign were produced with gate areas of 0.04 in^2 for the 0.5 and 0.375 inch bars and 0.016 in^2 for the 0.25 inch bars.

The die casting alloy used to produce the tensile bars was a modified 383 aluminum alloy of the composition given in Table I.

Table I: Alloy Composition

Element	Weight Percent
Silicon (Si)	12.019
Copper (Cu)	3.122
Iron (Fe)	0.911
Zinc (Zn)	2.516
Manganese (Mn)	0.183
Magnesium (Mg)	0.122
Tin (Sn)	0.04
Lead (Pb)	0.086
Nickel (Ni)	0.076
Chromium (Cr)	0.066
Titanium (Ti)	0.04
Bismuth (Bi)	0.033
Berylium (Be)	0.002
Lithium (Li)	0.001
Stronium (Sr)	0.003
Aluminum (Al)	80.819 (balance)

A 600 ton Lester die casting machine (Briggs & Stratton Station 59) was used for this campaign. The machine setup conditions are in Table II.

Table II: Machine Setup Conditions for February 27th 2003 B&S Campaign

Parameter	Value
Slow Shot Velocity (ips)	8.25-8.47
Fast Shot Velocity (ips)	31.5-33.65
Fast Shot Shift point (ips)	13.7-13.8
Delay after Pour (s)	1-9
Total Cycle Time (s)	30-43
Injection (holding) Pressure (psi)	1600
Shot Beads (g)	0.6
Biscuit Length (in)	0.70-0.89
Squeeze Distance (in)	0.12-0.31
Gate Thickness (in)	0.08
Gate Velocity (fps)	108-119
Cavity Fill Time (s)	0.048-0.043
Maximum Pressure (psi)	1572-1608
Intensification Delay (ms)	81-112
Metal Pressure (psi)	6000
Incoming Water Temperature (^{o}F)	80
System Pressure (psi)	1800
Tonnage Used	135
Incoming Water (psi)	25
Shot Pump Pressure (psi)	1500
Nitrogen Pressure (psi)	700
Accumulator Pressure (psi)	1000
Die Preheat Temperature (^{o}F)	125-150
Runner and Biscuit Preheat Temperature (^{o}F)	175

Experimental Campaign Conditions

The main objective of this study was to die cast tensile bars of a 383 aluminum alloy with varying amounts of ESP. Since the amount of ESP was anticipated to increase with increasing dwell time in the shot sleeve and lower metal pouring and shot sleeve temperatures, the three process variables chosen in this study were shot delay time, metal pouring temperature, and shot sleeve temperature. A water cooling line that could be turned on and off was used to try and control the shot sleeve temperature. Castings were produced for each of the experimental conditions given in Table III.

Table III: Experimental Campaign Conditions

Condition	Metal Temperature (^{o}F)	Shot Sleeve Temperature (Coil Water On/Off)	Shot Delay (s)
1	1270+/-20	On	1
2	1270+/-20	On	3
3	1270+/-20	On	6
4	1270+/-20	On	9
5	1270+/-20	Off	9
6	1270+/-20	Off	6
7	1270+/-20	Off	3
8	1270+/-20	Off	1
9	1270+/-20	On	1
10	1160+/-20	On	1
11	1160+/-20	On	3
12	1160+/-20	On	6
13	1160+/-20	Off	6
14	1160+/-20	Off	3
15	1160+/-20	Off	1

Ten shots were produced before each condition to allow the shot sleeve and die to reach the quasi-steady state thermal condition. A total of 299 die castings of the type in Figure 1 were produced at 1270^{o}F and 188 of these die castings were produced at 1160^{o}F. These numbers include the samples produced within the conditions that were saved, and the transition samples that were discarded. Condition 9 had the same setup conditions as condition 1 and was used to check for reproducibility in the tensile tests performed on the samples.

Process Variable Results

The furnace temperature of the aluminum alloy used during the campaign was measured throughout the campaign and is plotted for each shot number in Figure 4.

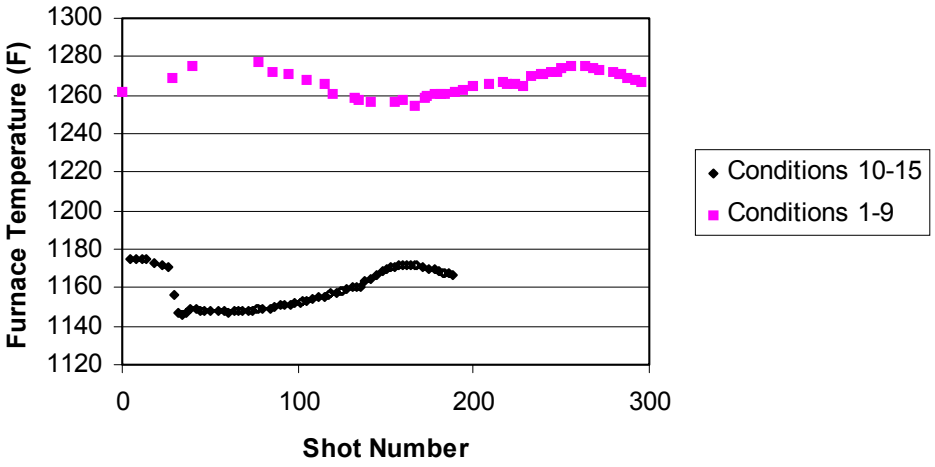

Figure 4: Metal Pour Temperature

The average furnace temperature throughout conditions 1-9 was 1267^{o}F with a standard deviation of 6 F, and conditions 10-15 had a furnace temperature of 1159 F with a standard deviation of 10 F. Thus there was a distinct high and low metal pour temperature in the campaign. However, the shot sleeve temperature was not found to vary throughout the campaign as can be seen in Figure 5.

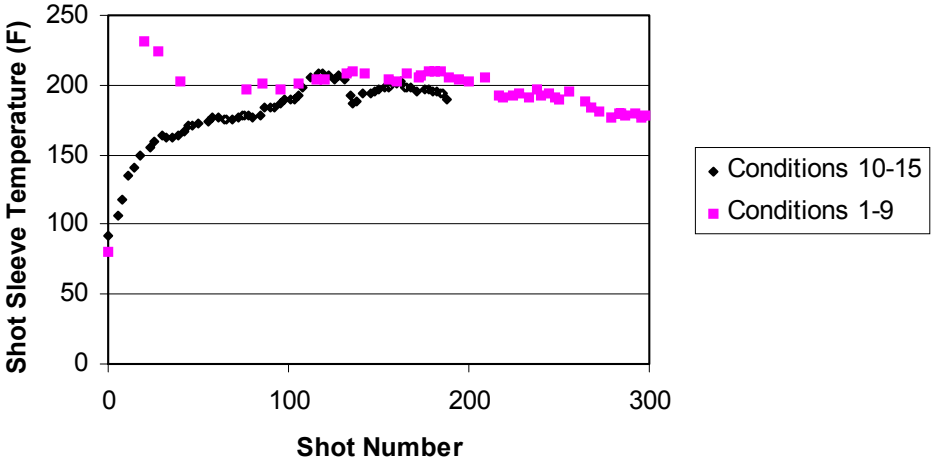

Figure 5: Shot Sleeve Temperature

Tensile Test Results

Room temperature tensile tests were performed on the samples under the guidelines set forth in the ASTM Standard for Tensile Testing of Metallic Materials E-8 (1). An Instron Model 1322 test frame was used with a crosshead velocity of 8×10^{-4} inches per second. An Epsilon extensometer was used, and data were scanned 25 times per second for a total of 2000 data points. The yield strength (0.2% offset), ultimate tensile strength (UTS), and fracture strain were determined and recorded for each tensile bar. Data analysis of the tensile data was done in Microsoft Excel and Minitab software packages. 2-sample t-tests were run on the sets of data to determine if the sample means were statistically different. A t value greater then 2.5 was used to determine that the samples were statistically different. Reproducibility checks of all three size tensile bars were performed and the results of the check are given in Table IV. The two conditions used for the check were conditions one and nine, which had metal pour temperatures of 1270°F, shot delay times of 1 second, and had the copper cooling lines for the shot sleeve turned on.

Table IV: Reproducibility Check

Condition	Bar Diameter (in)	Number of Samples	Property	Weibull Scale (50%)	Weibull Shape	t
1	0.25	15	Fracture Strain	0.0181	4.45	0.66
1	0.25	15	UTS (ksi)	38.6	13.01	1.61
1	0.25	15	Yield Strength (0.2% offset) (ksi)	22.9	29.84	1.39
9	0.25	10	Fracture Strain	0.019	5.9	
9	0.25	10	UTS (ksi)	40.2	18.99	
9	0.25	10	Yield Strength (0.2% offset) (ksi)	23.2	57.25	
1	0.375	19	Fracture Strain	0.0209	8.23	1.72
1	0.375	19	UTS (ksi)	40.3	22.81	0.16
1	0.375	19	Yield Strength (0.2% offset) (ksi)	21	49.91	1.43
9	0.375	10	Fracture Strain	0.0189	14.03	
9	0.375	10	UTS (ksi)	39	31.18	
9	0.375	10	Yield Strength (0.2% offset) (ksi)	20.9	53.35	
1	0.5	15	Fracture Strain	0.0145	6.01	0.59
1	0.5	15	UTS (ksi)	34.1	13.73	0.82
1	0.5	15	Yield Strength (0.2% offset) (ksi)	20.7	27.20	0.7
9	0.5	11	Fracture Strain	0.015	5.87	
9	0.5	11	UTS (ksi)	34.5	19.20	
9	0.5	11	Yield Strength (0.2% offset) (ksi)	20.8	40.45	

All three size tensile bars had t values less then 2.5 for yield strength, UTS, and fracture strain. As a result, statistically the tensile properties for the two equivalent conditions

were found to be members of the same data set. This proved that the die cast machine reproduced the specified conditions listed in Table III and produced equivalent samples throughout the campaign.

Fracture strain and UTS were found to decrease with an increase in shot delay time and/or decrease in temperature. The high and low temperature fracture strain and UTS results can be seen in Figures 6-9. A summary of all of the tensile properties for the three different size bars can be seen in the attached appendix.

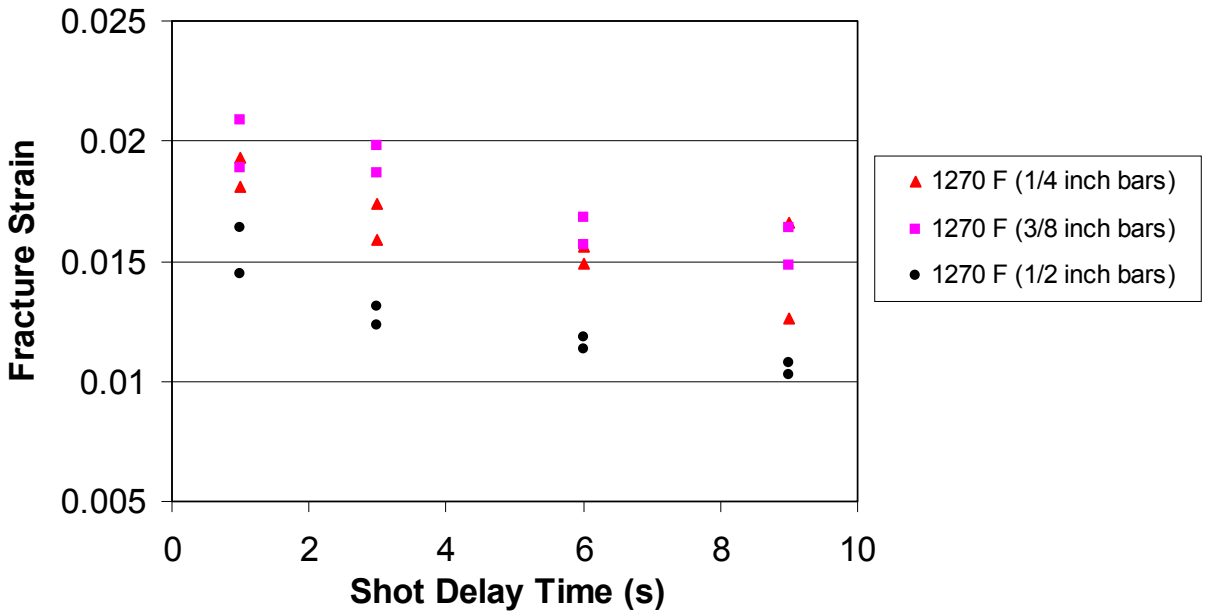

Figure 6: Fracture Strain Results at 1270°F

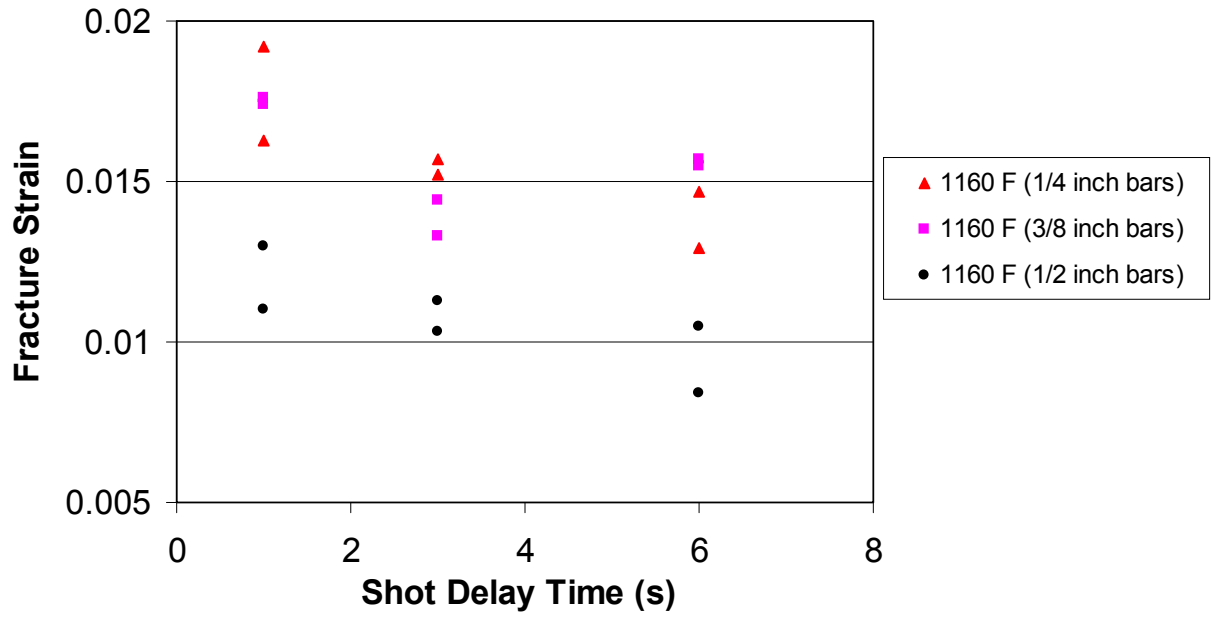

Figure 7: Fracture Strain Results at 1160°F

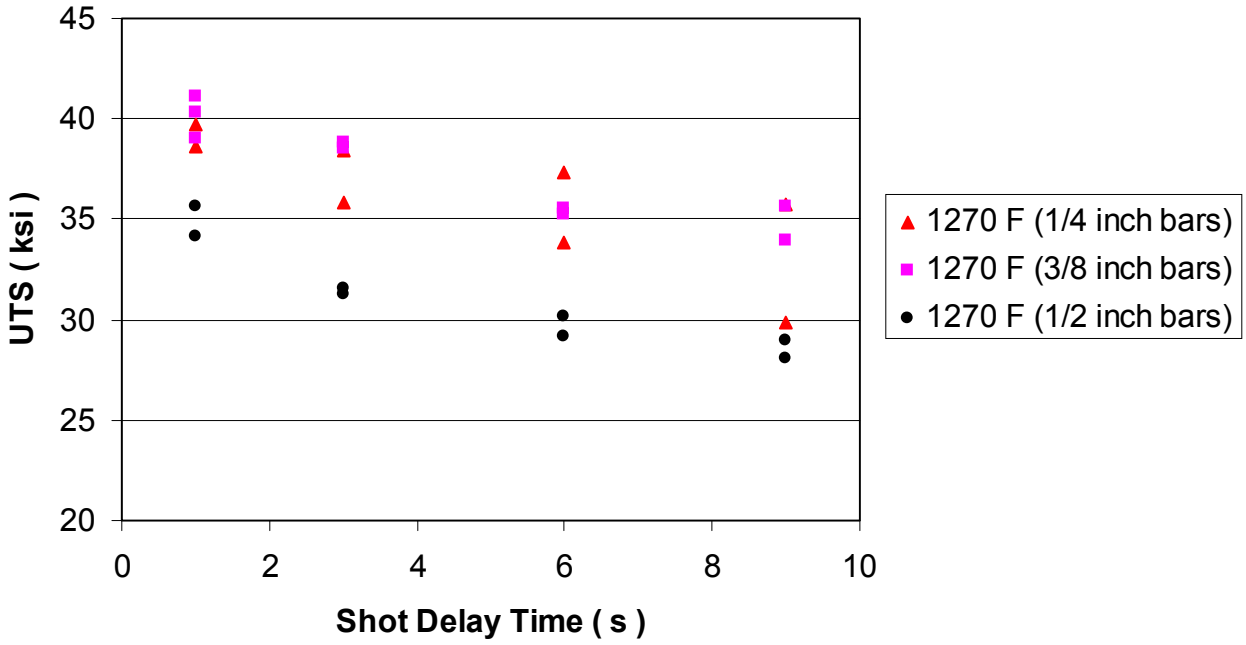

Figure 8: UTS Results at 1270°F

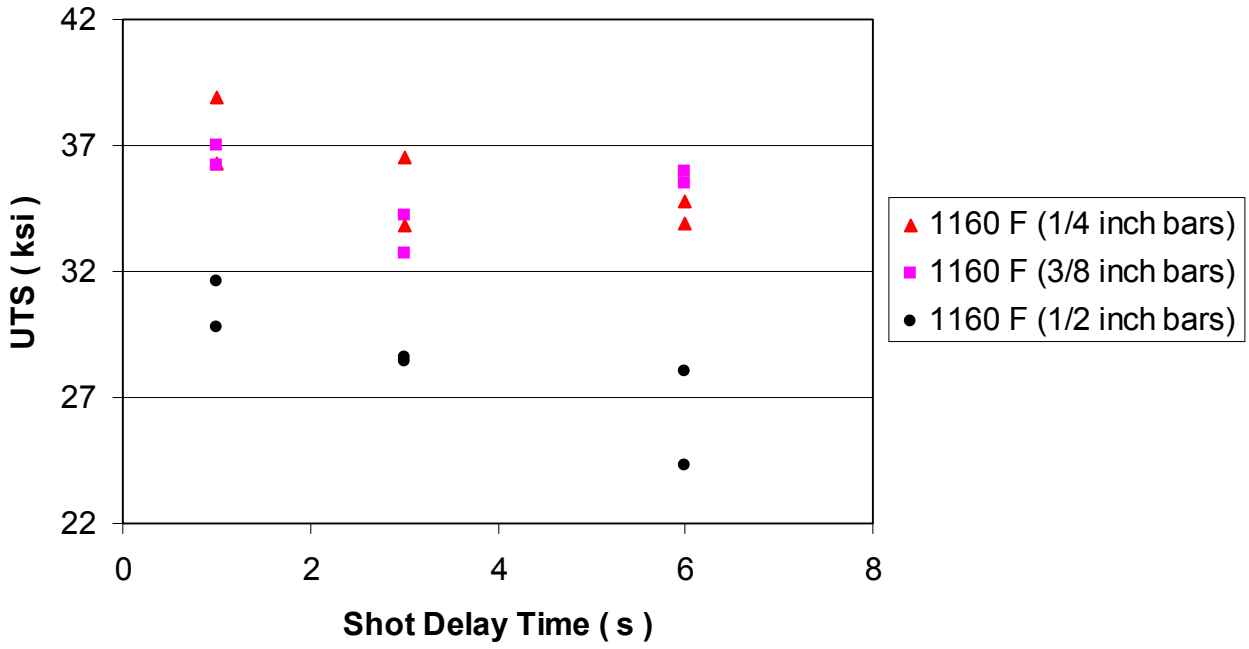

Figure 9: UTS Results at 1160°F

The decrease in fracture strain and UTS with an increase in shot delay time and/or decrease in metal pour temperature is believed to be a result of a combination of an increase in the volume fraction of ESP, an increased porosity level, a greater oxide content, and an increased occurrence of cold shuts.

A linear correlation was found between fracture strain and UTS. Figure 10 displays how UTS increases linearly with an increase in fracture strain. The tensile data from the 0.5 inch bars was used in Figure 10 to demonstrate the linear trend in fracture strain and UTS, but the 0.25 and 0.375 inch bars follow the same linear trend.

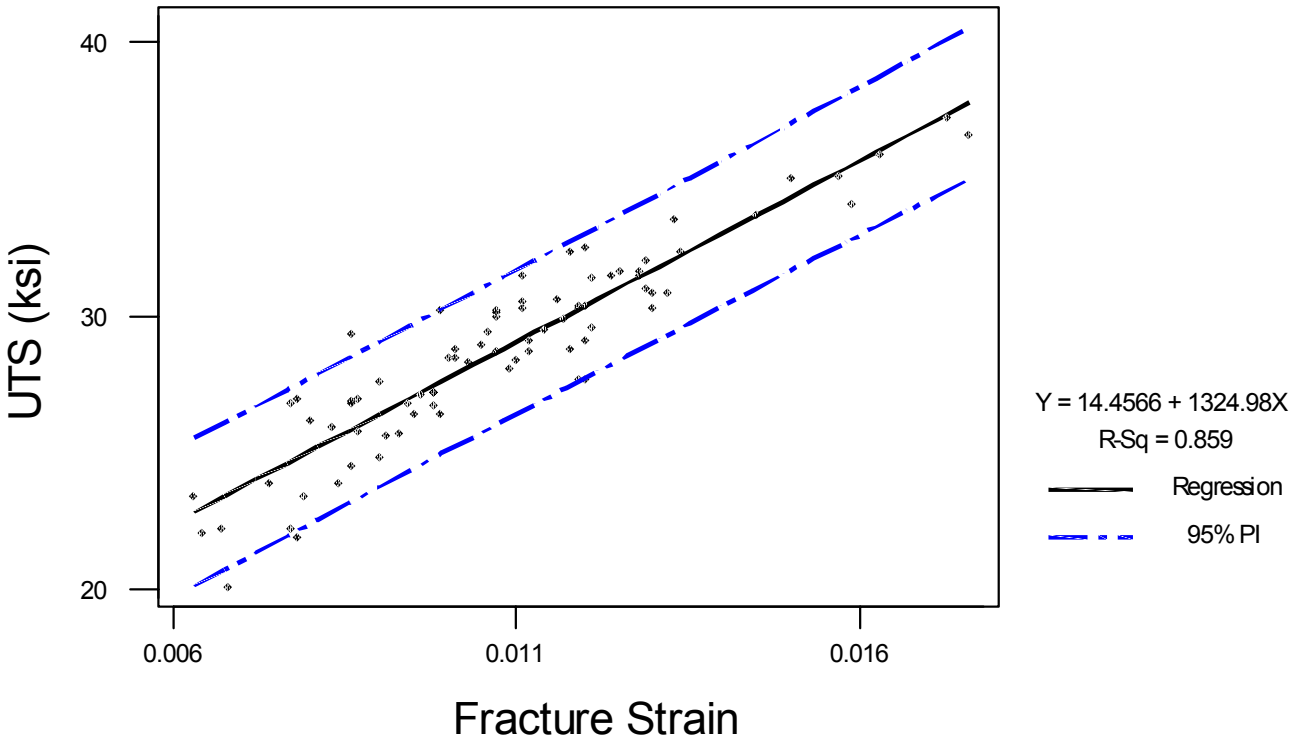

Figure 10: Correlation between Fracture Strain and UTS in 0.5 inch Tensile Bars

Weibull probability plots of fracture strain and UTS in conditions 1 and 10 of the 0.375 inch bars can be seen in Figures 11 and 12, respectively. Condition 1 had a metal pour temperature of 1270 °F, 1 second shot delay, and the water cooling line on, and condition 10 had a metal pour temperature of 1160 °F, 1 second shot delay, and the water cooling line on. These figures are representative of this campaign in displaying the decrease in fracture strain and UTS with a lower metal pour temperature.

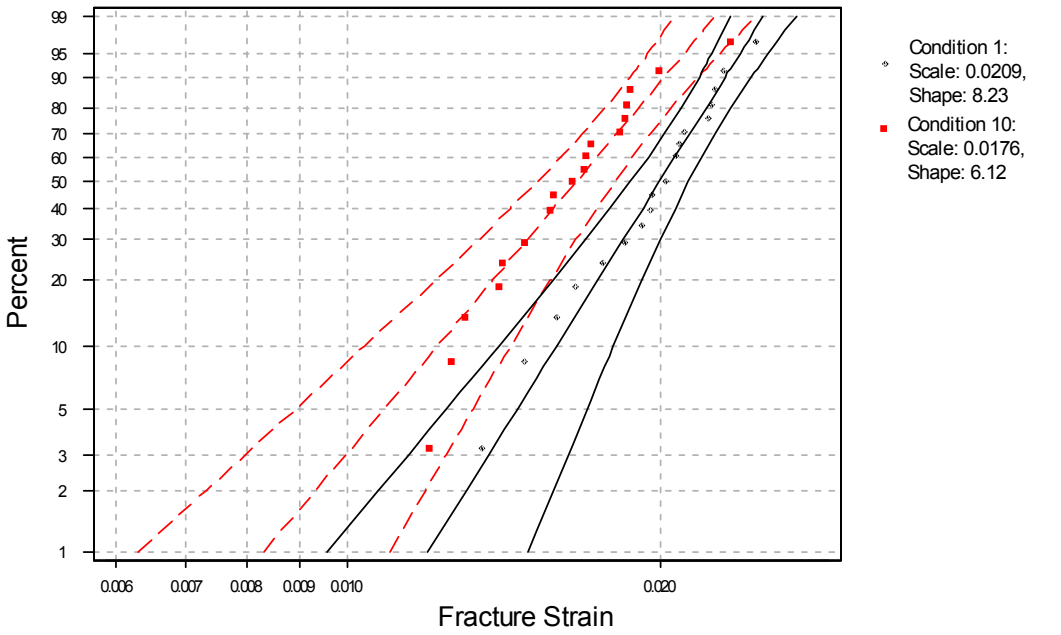

Figure 11: Weibull Probability Plot of Fracture Strain

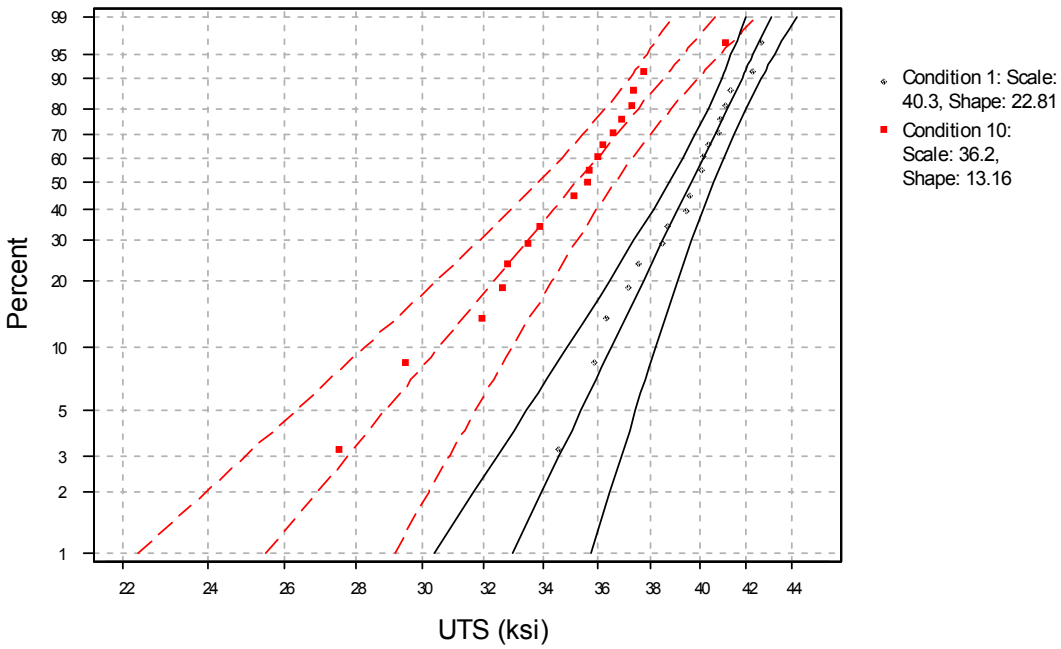

Figure 12: Weibull Probability Plot of UTS

Since yield strength is an inherent material property, the yield strength should be independent of volume fraction of ESP. The yield strength for all three size tensile bars in all fifteen conditions remained essentially constant. The yield strength was found to be 21 ± 2 ksi, which is in agreement with the ASTM standard (B85-02) value of 22 ksi for 0.25 inch diameter tensile samples (2). The yield strength found for all three size bars can be seen in Figure 13.

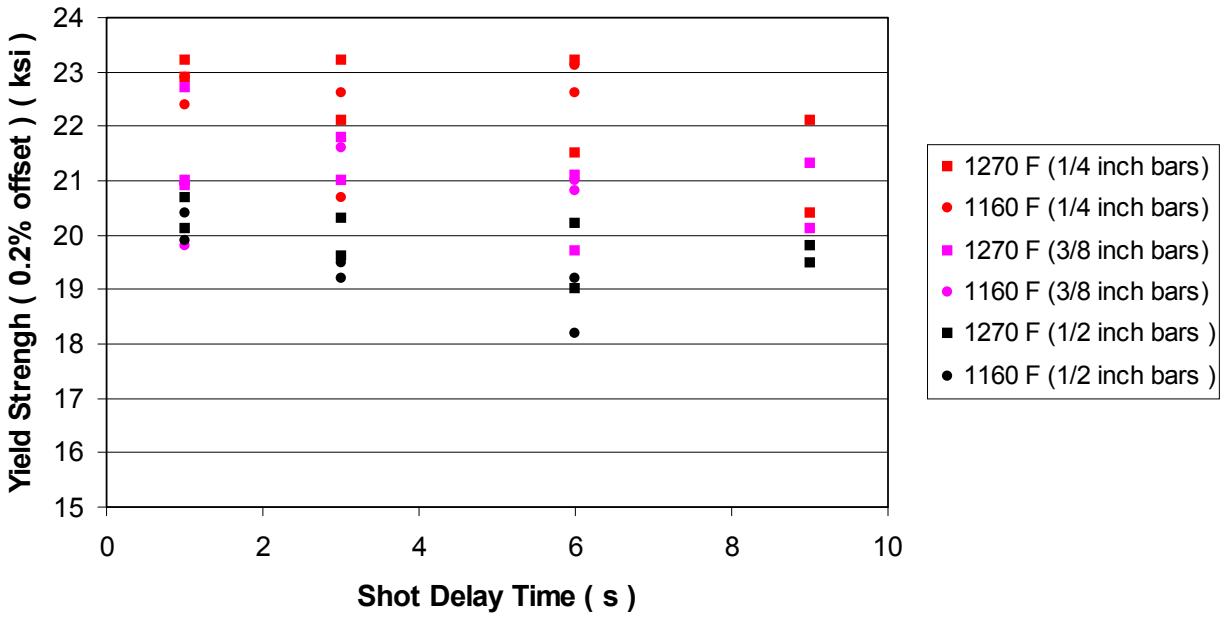

Figure 13: Yield Strength Results

Fracture Strain and UTS Comparison within each Tensile Bar Size

The fracture strain and UTS values were analyzed between conditions within each tensile bar size. 2-sample t-tests were used to determine if the individual data sets from each condition statistically belonged to the same data set. The 0.375 and 0.5 inch diameter bars were found to have t values that increased with decreasing metal pour temperature and/or increasing shot delay time. Statistically this resulted in the data from the two tensile bar sizes becoming two distinct data sets as the metal pour temperature increased and/or the shot delay time increased. The 0.25 inch diameter bars were found to have t values increase only with shot delay time in the high temperature conditions. The t-test results can be seen in Table V.

Table V: Summary of T-test Results

Conditions	Bar Diameter (in)	Property	Weibull Scales (50%)	t
1 vs. 2	0.25	Fracture Strain	0.0181 / 0.0159	1.15
1 vs. 3	0.25	Fracture Strain	0.0181 / 0.0149	1.78
1 vs. 4	0.25	Fracture Strain	0.0181 / 0.0126	2.84
1 vs. 10	0.25	Fracture Strain	0.0181 / 0.0163	1.06
2 vs. 11	0.25	Fracture Strain	0.0159 / 0.0157	0.49
3 vs. 12	0.25	Fracture Strain	0.0149 / 0.0129	1.26
1 vs. 2	0.25	UTS	38.6 / 35.8	1.64
1 vs. 3	0.25	UTS	38.6 / 33.8	3.32
1 vs. 4	0.25	UTS	38.6 / 29.9	5.9
1 vs. 10	0.25	UTS	38.6 / 36.3	1.64
2 vs. 11	0.25	UTS	35.8 / 36.5	0.81
3 vs. 12	0.25	UTS	33.8 / 33.9	0.13
1 vs. 2	0.375	Fracture Strain	0.0209 / 0.0187	2.16
1 vs. 3	0.375	Fracture Strain	0.0209 / 0.0168	3.63
1 vs. 4	0.375	Fracture Strain	0.0209 / 0.0148	4.7
1 vs. 10	0.375	Fracture Strain	0.0209 / 0.0176	3.45
2 vs. 11	0.375	Fracture Strain	0.0187 / 0.0144	3.42
3 vs. 12	0.375	Fracture Strain	0.0168 / 0.0155	0.9
1 vs. 2	0.375	UTS	40.3 / 38.8	2.03
1 vs. 3	0.375	UTS	40.3 / 35.2	4.68
1 vs. 4	0.375	UTS	40.3 / 33.9	5.51
1 vs. 10	0.375	UTS	40.3 / 36.2	5.13
2 vs. 11	0.375	UTS	38.8 / 34.2	4.25
3 vs. 12	0.375	UTS	35.2 / 35.5	0.51
1 vs. 2	0.5	Fracture Strain	0.0145 / 0.0131	1.21
1 vs. 3	0.5	Fracture Strain	0.0145 / 0.0118	2.84
1 vs. 4	0.5	Fracture Strain	0.0145 / 0.0103	4.03
1 vs. 10	0.5	Fracture Strain	0.0145 / 0.0110	4.01
2 vs. 11	0.5	Fracture Strain	0.0131 / 0.0103	4.24
3 vs. 12	0.5	Fracture Strain	0.0118 / 0.0084	5.3
1 vs. 2	0.5	UTS	34.1 / 31.6	2.17
1 vs. 3	0.5	UTS	34.1 / 29.2	4.73
1 vs. 4	0.5	UTS	34.1 / 28.1	4.83
1 vs. 10	0.5	UTS	34.1 / 29.8	4.48
2 vs. 11	0.5	UTS	31.6 / 28.4	3.51
3 vs. 12	0.5	UTS	29.2 / 24.3	5.72

Fracture Strain Comparison Between Tensile Bar Sizes

The fracture strains in the three different size tensile bars were compared by running 2-sample t-tests. The 0.25 and 0.375 inch diameter bars had t values less then 2.5 for their low and high temperature conditions. It was determined from these tests that 0.25 and 0.375 inch diameter bars have fracture strains that are statistically members of the same data set. The 0.25 and 0.5 inch diameter bars had t values less then 2.5 for the high temperature conditions, but t values higher then 2.5 for the low temperature conditions. As a result, the 0.25 and 0.5 inch diameter bars were only found to have fracture strains that were statistically members of the same data set at the high temperature conditions. The 0.375 and 0.5 inch diameter bars were found to have t values greater then 2.5 for both the high and low temperature conditions. As a result, the 0.375 and 0.5 inch diameter bars have fracture strains that are statistically members of different data sets. A summary of the 2-sample t-test results can be seen in Table VI.

Table VI: Tensile Bar Size Comparison

Conditions	Bar Diameters (in)	Weibull Scales (50%)	t
1 vs. 1	0.25 / 0.375	0.0181 / 0.0209	2.32
1 vs. 1	0.25 / 0.5	0.0181 / 0.0145	2.31
2 vs. 2	0.25 / 0.375	0.0159 / 0.0187	2.12
2 vs. 2	0.25 / 0.5	0.0159 / 0.0131	1.33
3 vs. 3	0.25 / 0.375	0.0149 / 0.0168	1.42
3 vs. 3	0.25 / 0.5	0.0149 / 0.0118	2.26
4 vs. 4	0.25 / 0.375	0.0126 / 0.0148	1.18
4 vs. 4	0.25 / 0.5	0.0126 / 0.0103	1.3
10 vs. 10	0.25 / 0.375	0.0163 / 0.0176	1.31
10 vs. 10	0.25 / 0.5	0.0163 / 0.0110	4.33
11 vs. 11	0.25 / 0.375	0.0157 / 0.0144	1.61
11 vs. 11	0.25 / 0.5	0.0157 / 0.0103	9.53
12 vs. 12	0.25 / 0.375	0.0129 / 0.0155	2.38
12 vs. 12	0.25 / 0.5	0.0129 / 0.0084	3.51
1 vs. 1	0.375 / 0.5	0.0209 / 0.0145	6.59
2 vs. 2	0.375 / 0.5	0.0187 / 0.0131	6.5
3 vs. 3	0.375 / 0.5	0.0168 / 0.0118	4.53
4 vs. 4	0.375 / 0.5	0.0148 / 0.0103	3.04
10 vs. 10	0.375 / 0.5	0.0176 / 0.0110	7.92
11 vs. 11	0.375 / 0.5	0.0144 / 0.0103	2.79
12 vs. 12	0.375 / 0.5	0.0155 / 0.0084	9.74

Observations and Conclusions Based on the Three Year Duration Study

The following observations and conclusions were formulated as a result of this study. Observations and conclusions 1 through 10 were developed from the results of the Flow3D computer simulations and the physical analog systems.

1. The liquid wave patterns in shot sleeves and the amount of air entrapped depend mainly on the plunger velocity and acceleration (plunger history).

2. At high plunger velocity, air is entrapped due to wave curling of wave in front of the plunger, and at low plunger velocity, air is entrapped by the waves reflected from the wall near the runner.

3. As the plunger acceleration increases about a critical value, the amount of air entrapped increases, because the waves start to curl earlier, and tend to curl with smaller curvature.

4. The effect of surface tension on the wave pattern and the amount of air entrapped is relatively small compared to the effect of the plunger history.

5. When the plunger velocity is large enough to cause wave curl, the surface tension tends to prevent the curling of the wave.

6. As the surface tension increases, the entrapped air decreases at plunger velocities greater than critical slow shot velocity.

7. At the same plunger velocity and acceleration, liquid wave patterns remain identical for constant kinematic viscosities.

8. The solid fraction present in the shot sleeve increases linearly with shot delay time.

9. For the range of heat transfer coefficients normally associated with shot sleeves, the solid fraction in the shot sleeve is relatively constant (independent of the heat transfer coefficient).

10. The wave pattern remaining after filling the shot sleeve significantly influences and alters the wave pattern generated by the plunger motion.

Observations 11 through 16 were developed through the characterizations of the aluminum die castings produced in the Briggs & Stratton Corp. die casting campaigns.

11. The yield strengths of the die cast modified 383 aluminum alloy were essentially constant, independent of the alloy pour temperature and the shot delay times.

12. The ultimate tensile strengths, fracture elongations, and fatigue properties were dependent on the alloy pour temperatures and shot delay times.

13. The ultimate tensile strength and fracture elongation decreased as the alloy pour temperature decreased and the shot delay time increased.

14. For this limited ductility alloy, the ultimate tensile strength increased linearly with the fracture elongation.

15. Weibull statistics should be used to report the ultimate tensile strength and fracture elongation data for these limited ductility products, as the distribution of these properties were not Gaussian.

16. The ultimate tensile strengths and fracture elongation values recorded for the components and tensile bars die cast in this project were significantly less than those reported for this alloy in the NADCA Product Specification Standards for Die Castings.

17. The occurrence of ESP and fluidity-related defects significantly reduces the ultimate tensile strengths and fracture elongation for these limited ductility products.

18. Micro-gaps exist between the eutectic silicon platelets in the ESP and matrix interface which may provide permeability paths and/or crack initiation sites.

An observation and conclusion based on the Briggs & Stratton Corp die casting campaign and analysis of the energy usage in the die casting process is as follows:

19. Significant energy savings is available by reducing the average pour weight in the die casting process. The measured range of pour weights were typically ± 5 % in several die casting facilities. A manufacture of robotic ladling devices quotes set up ranges of pour weight as between ± 0.5 to 2 %, depending on the specific unit used. The elimination of the larger than average pour weights would not alter the acceptability of the die cast components and would significantly decrease the amount of materials used and, accordingly, the energy used per product.

Project Reporting, Publications and Student Participants

During the first year of this project a web page was established to provide timely reporting of the project activities and accomplishments to the Sponsors, NADCA technical monitors, and the public. The address of the web page is www.mse.eng.ohio-state.edu/~mobley/diecasting/html. That web page has been updated throughout the life of this project to include ongoing project activities and findings.

In addition to providing reports of the project activities on the web page, oral reports of the project activities were presented and reviewed at the following North American Die Casting Association (NADCA) Committee and Chapter meetings:

NADCA Committee/Group	Meeting Date	Meeting Place
Computer Modeling	8/29/2000	OSU, Columbus, OH
R&D	9/13/2000	NADCA, Illinois
Technical Process	11/13/2000	OSU, Columbus, OH
Computer Modeling	12/7/2000	OSU, Columbus, OH
R&D	2/7/2001	NADCA, Illinois
Computer Modeling	4/25/2001	OSU, Columbus, OH
Technical Process	6/14/2001	GM, Bedford, IN
R&D	6/20/2001	OSU, Columbus, OH
Computer Modeling	9/13/2002	OSU, Columbus, OH
R&D	9/25/2001	OSU, Columbus, OH
Congress & Exposition	10/29-11/1/2001	Cincinnati, OH
Computer Modeling	12/11/2002	OSU, Columbus, OH
Milwaukee Chapter	2/27/2002	Milwaukee, WI
Computer Modeling	4/24/2002	OSU, Columbus, OH
R&D	6/12/2002	Case Western Reserve University, Cleveland, OH
Congress & Exposition	9/30 & 10/2/2002	Rosemont, IL
R&D	1/23/2003	NADCA, Illinois
Computer Modeling	4/23/2003	OSU, Columbus, OH
R&D	6/26/2003	Colorado School of Mines Golden, CO

Based on the results of the first year's activities, one paper titled "Mircrostructural Features in Aluminum Alloy Die Castings" was submitted and presented at NADCA's International Die Casting Congress and Exposition held in Cincinatti, Ohio in October, 2001. Based on the results of the second year's activities, two papers titled "3-Dimensional Simulation of Melt Flow in Die Casting Shot Sleeves" and "The Effects of Shot Delay Time on the Microstructures and Mechanical Properties of a Die Cast Aluminum Alloy" were presented at NADCA's International Die Casting Congress and Exposition held in Chicago, Illinois on September 30 through October 2, 2002. A fourth manuscript, titled "The Effects of Externally Solidified Product and Flow Defects on the Tensile Properties of an Aluminum Die Casting Alloy" is to be submitted to both NADCA and the American Foundry Society (AFS) for publication.

A total of four students worked on this project. Tao Liang, who worked on correlating the microstructural features of the aluminum die castings with their mechanical properties, completed the requirements for the M.S. Degree at the end of the Summer Quarter, 2002. Mr. Liang is continuing his graduate studies pursuing a Ph.D. Degree in OSU's Materials Science and Engineering Program. Junmin Park, who worked on the computer modeling of the wave phenomena in the shot sleeve, successfully passed the Ph.D. candidacy exam during the Spring Academic Quarter, 2002. At the end of the 2003 Summer Quarter, Mr. Park elected to leave the OSU Graduate Program. Doug Pohlman is a BS/MS student majoring in the Materials Science & Engineering Department. He worked on the effects of ESP on the mechanical properties of die cast aluminum alloys as part of his Senior Research Project. Doug is expected to graduate with a BS/MS Degree by the Spring of 2004. Tim Hider, an undergraduate Senior majoring in the Materials Science and Engineering Department, began working on the project during the Summer Quarter, 2002 and graduated with a BS Degree June, 2003. His Senior Research Project was based on the physical analog modeling of wave formation in transparent shot sleeves under athermal conditions. After graduation with the BS Degree, Mr. Hider took full time employment with Honda of American in their Anna casting facilities.

References

1. ASTM, 1969 Book of ASTM Standards, Part 31: Physical and Mechanical Testing of Metals – Metallurgraphy, Nondestructive Testing, Fatigue, Effect of Temperature, American Society for Testing and Materials, 1969, E8, 205-206.

2. ASTM, 2002 Book of ASTM Standards, Section 2: Nonferrous Metal Products, Volume 02.02: Aluminum and Magnesium Alloys, American Society for Testing and Materials, 2002, B85, pg. 32.

Appendix 1: Summary of Tensile Test Results for 0.25 inch Tensile Bars

Condition	Number of Samples	Property	Average	Stdev	Weibull Scale (50%)	Weibull Shape
1	15	Fracture Strain	0.0165	0.004	0.0181	4.45
1	15	UTS (ksi)	37	4	38.6	13.01
1	15	Proportional Limit (ksi)	14.1	2	14.7	14.53
1	15	Yield Strength (0.2% offset) (ksi)	22.4	2	22.9	29.84
2	9	Fracture Strain	0.0144	0.004	0.0159	3.66
2	9	UTS (ksi)	34	5	35.8	10.06
2	9	Proportional Limit (ksi)	12.5	2.4	13.4	7.35
2	9	Yield Strength (0.2% offset) (ksi)	21.1	2.6	22.1	11.22
3	9	Fracture Strain	0.0137	0.003	0.0149	5.66
3	9	UTS (ksi)	32.4	3	33.8	12.10
3	9	Proportional Limit (ksi)	12.1	3	13.2	5.61
3	9	Yield Strength (0.2% offset) (ksi)	20.4	2.6	21.5	10.17
4	6	Fracture Strain	0.0115	0.003	0.0126	4.10
4	6	UTS (ksi)	28.8	2.5	29.9	12.44
4	6	Proportional Limit (ksi)	12	2.4	12.9	6.33
4	6	Yield Strength (0.2% offset) (ksi)	19.5	2	20.4	11.82
5	8	Fracture Strain	0.0149	0.005	0.0166	3.43
5	8	UTS (ksi)	33.3	6	35.7	6.72
5	8	Proportional Limit (ksi)	13	2	13.7	10.73
5	8	Yield Strength (0.2% offset) (ksi)	21.2	2	22.1	13.30
6	7	Fracture Strain	0.0145	0.003	0.0156	6.25
6	7	UTS (ksi)	36.1	3	37.3	18.44
6	7	Proportional Limit (ksi)	14.6	0.6	14.9	25.43
6	7	Yield Strength (0.2% offset) (ksi)	23.1	0.3	23.2	97.14
7	9	Fracture Strain	0.016	0.004	0.0174	4.75
7	9	UTS (ksi)	37	3	38.4	13.70
7	9	Proportional Limit (ksi)	15	1	15.3	23.43
7	9	Yield Strength (0.2% offset) (ksi)	22.8	1	23.2	38.80
8	6	Fracture Strain	0.0188	0.001	0.0193	17.11
8	6	UTS (ksi)	38.6	3	39.7	19.50
8	6	Proportional Limit (ksi)	14	5	15.6	3.65
8	6	Yield Strength (0.2% offset) (ksi)	21.9	3.6	23.2	8.71
9	10	Fracture Strain	0.0176	0.004	0.019	5.90
9	10	UTS (ksi)	39	2.5	40.2	18.99
9	10	Proportional Limit (ksi)	14.7	1	15.1	21.05
9	10	Yield Strength (0.2% offset) (ksi)	23	0.4	23.2	57.25
10	13	Fracture Strain	0.0149	0.004	0.0163	4.36
10	13	UTS (ksi)	35	3	36.3	12.90
10	13	Proportional Limit (ksi)	13	1.4	13.6	11.01
10	13	Yield Strength (0.2% offset) (ksi)	22.1	1	22.4	35.05
11	10	Fracture Strain	0.0151	0.001	0.0157	11.17
11	10	UTS (ksi)	35.4	2.5	36.5	16.70
11	10	Proportional Limit (ksi)	13.1	2	13.8	9.73
11	10	Yield Strength (0.2% offset) (ksi)	21.8	2	22.6	15.14
12	8	Fracture Strain	0.0118	0.003	0.0129	5.40
12	8	UTS (ksi)	32.1	5	33.9	10.13
12	8	Proportional Limit (ksi)	14.3	2	15	11.45
12	8	Yield Strength (0.2% offset) (ksi)	22.3	2	23.1	16.03
13	6	Fracture Strain	0.0138	0.002	0.0147	6.58
13	6	UTS (ksi)	33.3	3	34.8	11.35
13	6	Proportional Limit (ksi)	14.1	2.5	15	8.40
13	6	Yield Strength (0.2% offset) (ksi)	21.8	2.5	22.6	17.53
14	8	Fracture Strain	0.0139	0.003	0.0152	5.30
14	8	UTS (ksi)	32.1	4.5	33.8	10.59
14	8	Proportional Limit (ksi)	11	1	11.4	14.82
14	8	Yield Strength (0.2% offset) (ksi)	20.1	1.4	20.7	20.69
15	8	Fracture Strain	0.0181	0.003	0.0192	7.57
15	8	UTS (ksi)	38	2	38.9	19.90
15	8	Proportional Limit (ksi)	13	1.6	13.6	9.81
15	8	Yield Strength (0.2% offset) (ksi)	22.2	1.4	22.9	17.14

Appendix 2: Summary of Tensile Test Results for 0.375 inch Tensile Bars

Condition	Number of Samples	Property	Average	Stdev	Weibull Scale (50%)	Weibull Shape
1	19	Fracture Strain	0.0197	0.003	0.0209	8.23
1	19	UTS (ksi)	39.4	2	40.3	22.81
1	19	Proportional Limit (ksi)	9.8	1	10.1	12.96
1	19	Yield Strength (0.2% offset) (ksi)	20.7	1	21	49.91
2	15	Fracture Strain	0.0177	0.002	0.0187	8.48
2	15	UTS (ksi)	37.9	2	38.8	23.68
2	15	Proportional Limit (ksi)	10.7	1	11.03	20.27
2	15	Yield Strength (0.2% offset) (ksi)	21	0.4	21	76.64
3	12	Fracture Strain	0.0156	0.003	0.0168	6.39
3	12	UTS (ksi)	33.8	4	35.2	14.74
3	12	Proportional Limit (ksi)	9.9	2	10.6	7.34
3	12	Yield Strength (0.2% offset) (ksi)	19.2	1	19.7	20.83
4	9	Fracture Strain	0.0135	0.003	0.0148	4.38
4	9	UTS (ksi)	32.4	3	33.9	10.24
4	9	Proportional Limit (ksi)	11.8	2	12.5	9.27
4	9	Yield Strength (0.2% offset) (ksi)	19.7	1	20.1	24.72
5	12	Fracture Strain	0.015	0.004	0.0164	4.72
5	12	UTS (ksi)	34.5	2	35.6	15.06
5	12	Proportional Limit (ksi)	13.3	2	13.9	14.64
5	12	Yield Strength (0.2% offset) (ksi)	20.9	1	21.3	28.39
6	12	Fracture Strain	0.0146	0.003	0.0157	6.70
6	12	UTS (ksi)	34	4	35.5	12.97
6	12	Proportional Limit (ksi)	12.5	3	13.4	7.02
6	12	Yield Strength (0.2% offset) (ksi)	20.4	2	21.1	21.84
7	9	Fracture Strain	0.0187	0.003	0.0198	7.77
7	9	UTS (ksi)	37.7	2	38.5	24.41
7	9	Proportional Limit (ksi)	14.6	1	15	17.50
7	9	Yield Strength (0.2% offset) (ksi)	21.3	1	21.8	21.47
8	10	Fracture Strain	0.0213	0.004	0.0228	7.28
8	10	UTS (ksi)	40.3	2	41.1	31.63
8	10	Proportional Limit (ksi)	15.2	2	15.9	11.36
8	10	Yield Strength (0.2% offset) (ksi)	22.2	1	22.7	33.24
9	10	Fracture Strain	0.0184	0.002	0.0189	14.03
9	10	UTS (ksi)	38.4	2	39	31.18
9	10	Proportional Limit (ksi)	11.8	1	12	31.53
9	10	Yield Strength (0.2% offset) (ksi)	20.7	1	20.9	53.35
10	19	Fracture Strain	0.0165	0.003	0.0176	6.12
10	19	UTS (ksi)	34.9	3	36.2	13.16
10	19	Proportional Limit (ksi)	10.1	2	10.9	6.20
10	19	Yield Strength (0.2% offset) (ksi)	19.3	1	19.8	21.13
11	9	Fracture Strain	0.0131	0.003	0.0144	4.64
11	9	UTS (ksi)	33	3	34.2	15.39
11	9	Proportional Limit (ksi)	9.8	1	10.1	16.24
11	9	Yield Strength (0.2% offset) (ksi)	20.8	2	21.6	12.02
12	11	Fracture Strain	0.0147	0.002	0.0155	9.32
12	11	UTS (ksi)	34.4	2	35.5	19.55
12	11	Proportional Limit (ksi)	10.7	1	11.3	11.76
12	11	Yield Strength (0.2% offset) (ksi)	20.4	1	20.8	24.67
13	8	Fracture Strain	0.0153	0.002	0.0157	9.30
13	8	UTS (ksi)	34.7	3	36	15.56
13	8	Proportional Limit (ksi)	11.3	1	11.8	16.13
13	8	Yield Strength (0.2% offset) (ksi)	20.6	1	21	27.11
14	8	Fracture Strain	0.0123	1	0.0133	4.67
14	8	UTS (ksi)	31.5	3	32.7	13.20
14	8	Proportional Limit (ksi)	11.6	1	11.9	23.68
14	8	Yield Strength (0.2% offset) (ksi)	20.1	0.5	20.3	55.11
15	8	Fracture Strain	0.0164	0.002	0.0174	8.62
15	8	UTS (ksi)	36.3	2	37	25.40
15	8	Proportional Limit (ksi)	11.8	1	12	41.27
15	8	Yield Strength (0.2% offset) (ksi)	20.4	1	20.7	43.37

Appendix 3: Summary of Tensile Test Results for 0.5 inch Tensile Bars

Condition	Number of Samples	Property	Average	Stdev	Weibull Scale (50%)	Weibull Shape
1	15	Fracture Strain	0.0134	0.002	0.0145	6.01
1	15	UTS (ksi)	32.8	3	34.1	13.73
1	15	Proportional Limit (ksi)	11.7	2	12.4	8.60
1	15	Yield Strength (0.2% offset) (ksi)	20.3	1	20.7	27.20
2	10	Fracture Strain	0.0124	0.002	0.0131	7.97
2	10	UTS (ksi)	30.7	2	31.6	17.86
2	10	Proportional Limit (ksi)	9.8	1	10.2	13.54
2	10	Yield Strength (0.2% offset) (ksi)	19.2	1	19.6	37.22
3	10	Fracture Strain	0.0111	0.001	0.0118	8.91
3	10	UTS (ksi)	28.4	2	29.2	18.06
3	10	Proportional Limit (ksi)	10.4	1	10.8	11.67
3	10	Yield Strength (0.2% offset) (ksi)	18.8	0.6	19	30.66
4	8	Fracture Strain	0.0095	0.002	0.0103	5.31
4	8	UTS (ksi)	26.9	3	28.1	11.78
4	8	Proportional Limit (ksi)	9.6	0.6	9.9	18.75
4	8	Yield Strength (0.2% offset) (ksi)	19.1	1	19.5	27.85
5	10	Fracture Strain	0.01	0.002	0.0108	5.29
5	10	UTS (ksi)	27.8	2.7	29	12.65
5	10	Proportional Limit (ksi)	12	1.4	12.6	11.06
5	10	Yield Strength (0.2% offset) (ksi)	19.6	0.6	19.8	42.27
6	11	Fracture Strain	0.0108	0.001	0.0113	11.30
6	11	UTS (ksi)	29.4	1.6	30.2	19.71
6	11	Proportional Limit (ksi)	12	1	12.5	12.02
6	11	Yield Strength (0.2% offset) (ksi)	19.9	0.6	20.2	37.39
7	12	Fracture Strain	0.0115	0.002	0.0123	8.13
7	12	UTS (ksi)	30.4	2.3	31.3	19.85
7	12	Proportional Limit (ksi)	11.6	2	12.4	8.21
7	12	Yield Strength (0.2% offset) (ksi)	19.8	1	20.3	25.31
8	10	Fracture Strain	0.0149	0.004	0.0164	4.63
8	10	UTS (ksi)	34.1	3.6	35.6	12.92
8	10	Proportional Limit (ksi)	11.1	1.3	11.7	11.66
8	10	Yield Strength (0.2% offset) (ksi)	19.9	0.4	20.1	67.48
9	11	Fracture Strain	0.014	0.002	0.015	5.87
9	11	UTS (ksi)	33.6	2	34.5	19.20
9	11	Proportional Limit (ksi)	12.4	1.3	12.9	12.96
9	11	Yield Strength (0.2% offset) (ksi)	20.5	0.6	20.8	40.45
10	16	Fracture Strain	0.0103	0.002	0.011	8.78
10	16	UTS (ksi)	29.1	1.6	29.8	23.01
10	16	Proportional Limit (ksi)	9.9	0.6	10.2	17.16
10	16	Yield Strength (0.2% offset) (ksi)	19.7	0.4	19.9	48.28
11	12	Fracture Strain	0.0097	0.001	0.0103	7.57
11	12	UTS (ksi)	27.4	2.4	28.4	15.39
11	12	Proportional Limit (ksi)	9.5	1	9.9	13.04
11	12	Yield Strength (0.2% offset) (ksi)	19	1	19.5	27.30
12	9	Fracture Strain	0.0079	0.001	0.0084	7.60
12	9	UTS (ksi)	23.4	2	24.3	14.02
12	9	Proportional Limit (ksi)	9.4	1	9.8	13.16
12	9	Yield Strength (0.2% offset) (ksi)	17.9	1	18.2	35.18
13	7	Fracture Strain	0.0098	0.002	0.0105	7.09
13	7	UTS (ksi)	27	2	28	14.64
13	7	Proportional Limit (ksi)	9.9	0.6	10.2	17.43
13	7	Yield Strength (0.2% offset) (ksi)	18.8	0.6	19.2	31.86
14	8	Fracture Strain	0.0106	0.002	0.0113	8.21
14	8	UTS (ksi)	28	1.6	28.6	26.46
14	8	Proportional Limit (ksi)	10.7	2	11.4	7.33
14	8	Yield Strength (0.2% offset) (ksi)	18.3	2.6	19.2	13.96
15	8	Fracture Strain	0.012	0.002	0.013	6.05
15	8	UTS (ksi)	30.7	2	31.6	18.38
15	8	Proportional Limit (ksi)	12.7	1	13	20.38
15	8	Yield Strength (0.2% offset) (ksi)	20.1	0.6	20.4	39.70